HHS Public Access

Author manuscript

Cell Chem Biol. Author manuscript; available in PMC 2023 June 16.

Published in final edited form as:

Cell Chem Biol. 2022 June 16; 29(6): 985–995.e5. doi:10.1016/j.chembiol.2022.01.004.

Ligand-induced interactions between butyrophilin 2A1 and 3A1 internal domains in the HMBPP receptor complex

Chia-Hung Christine Hsiao[1],

Khiem Nguyen[1],

Yiming Jin[1],

Olga Vinogradova[1],

Andrew J. Wiemer[1,2,*]

[1]Department of Pharmaceutical Sciences, University of Connecticut, Storrs, Connecticut, 06269, USA

[2]Institute for Systems Genomics, University of Connecticut, Storrs, Connecticut, 06269, USA

Summary

Ligand-bound HMBPP receptor (BTN3A1 and BTN2A1) is detectable by the TCR of Vγ9Vδ2 T cells. While BTN3A1 binds to phosphoantigens, the mechanisms resulting in receptor activation are not clear. We used CRISPR/Cas9, ELISA, nano-BRET and ITC to evaluate the role of BTN2A1. Depletion of BTN2A1 and rescue experiments demonstrate that its internal domain is essential for pAg detection. Internal hetero-BRET signals are observed between BTN2A1 and BTN3A1, which are increased by pAg. ITC detects a direct interaction between the intracellular domains of BTN3A1 and BTN2A1, only in the presence of pAg. This interaction is abrogated by removal of the BTN2A1 JM region, but not by removal of the BTN3A1 JM region. Regional mutations between BTN2A1 316–326 clearly impact IFNγ response and hetero-BRET signal.

*Lead contact/correspondence: Andrew Wiemer, andrew.wiemer@uconn.edu, Twitter: @WiemerLab.

Author contributions

Conceptualization - A.W. and O.V.
Formal Analysis - A.W. and O.V.
Funding acquisition - A.W. and O.V.
Investigation - C.H., K.N., Y.J., A.W. and O.V.
Project administration -A.W. and O.V.
Resources - A.W. and O.V.
Supervision - A.W. and O.V.
Validation - C.H., K.N., Y.J.
Visualization - K.N. and A.W.
Writing – K.N., A.W. and O.V.
Writing – review & editing - C.H., K.N., Y.J., A.W. and O.V.

Declaration of interests

A.J.W. is a co-founder of Terpenoid Therapeutics. The current work did not involve the company. The other authors have nothing to declare.

Supplemental information

Supplemental Information includes three figures and one table and can be found with this article online at: https://doi.org/10.1016/j.chembiol.2022.01.004

Mutations to amino acids L318, W320, and L325 indicate these amino acids are crucial. Together, these studies demonstrate a pAg-inducible interaction between BTN2A1 and BTN3A1 internal domains.

Graphical Abstract

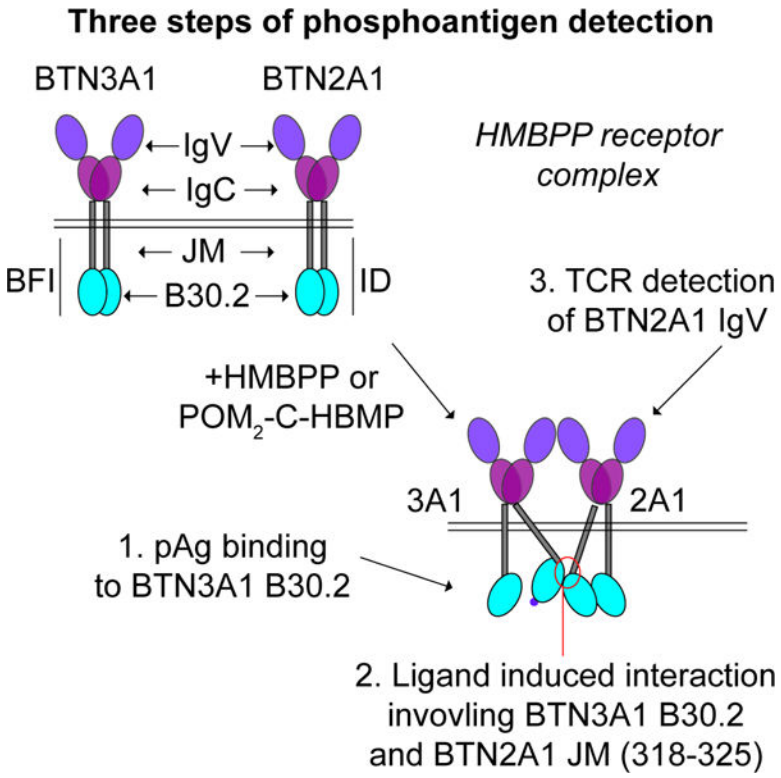

eTOC

Hsiao et al. identify and characterize a phosphoantigen dependent interaction between BTN2A1 and BTN3A1 internal domains which is necessary for the Vγ9Vδ2 T cell response to phosphoantigen. The interaction has been localized to a region in the BTN2A1 protein and amino acids that are required for function have been identified.

Introduction

Detection of antigens is central to the activation of T cells and the immune responses they coordinate. While most T cells use their T cell receptors (TCRs) to detect peptide antigens presented by the major histocompatibility complex (MHC), γδ T cells detect a wider variety of ligands (Willcox and Willcox, 2019). The largest blood population of γδ T cells, the Vγ9Vδ2 T cells, detect small phosphorus-containing molecules known as pAgs in a way that is independent of MHC (Morita et al., 2007). Understanding the unique mechanisms of pAg detection is critical because of various roles that Vγ9Vδ2 T cells play in detection of cancer, infectious disease, and inflammatory conditions (McCarthy and Eberl, 2018;

Vantourout and Hayday, 2013; Vermijlen et al., 2018). This may lead to new ways to therapeutically manipulate these cells to benefit human health.

In recent years, it has become clear that pAgs act through binding to the butyrophilin protein BTN3A1 (Harly et al., 2012; Hsiao et al., 2014; Riano et al., 2014; Sandstrom et al., 2014) (Figure 1). This includes natural pAgs such as (*E*)-4-hydroxy-3-methyl-but-2-enyl diphosphate (HMBPP) or its synthetic analogs such as bis (pivaloyloxymethyl) (*E*)-4-hydroxy-3-methyl-but-2-enyl phosphonate (POM_2-C-HMBP). Binding to BTN3A1 induces conformational and clustering changes in the protein, which can lead to detection by the Vγ9Vδ2 T cells (Hsiao et al., 2014). The internal B30.2 domain of BTN3A1 contains the pAg binding pocket, and ligand receptor interactions at this position are essential for pAg detection by the Vγ9Vδ2 T cells (Poe et al., 2019; Wiemer, 2020). BTN3A1 and the Vγ9Vδ2 TCR can participate in sensing of pAg-containing cells by the T cells (Hsiao and Wiemer, 2018). Or, these two receptors also can participate in self-activation of Vγ9Vδ2 T cells in the absence of any cell-to-cell contact (Laplagne et al., 2021). In addition to its role in activating Vγ9Vδ2 T cells, BTN3A1 has also been reported to function as a new immune checkpoint that impacts antigen dependent activation of traditional T cells (Payne et al., 2020).

While early models suggested that there might be direct interaction between BTN3A1 and the Vγ9Vδ2 TCR, evidence for this direct interaction is lacking (Gu et al., 2018). This suggests additional proteins are involved with pAg detection. Recent studies have determined that the related protein BTN2A1, though not capable of pAg binding, is also essential for the cellular response to pAgs (Karunakaran et al., 2020; Rigau et al., 2020). Unlike BTN3A1, direct interactions have been observed between BTN2A1 and the Vγ9Vδ2 TCR. Thus, BTN3A1 does not work alone, but rather BTN3A1 and BTN2A1 are part of an pAg receptor complex. As HMBPP is the most potent natural pAg, the BTN3A1/2A1 complex can also be referred to as the HMBPP receptor. It remains unclear how exactly BTN2A1 and BTN3A1 interact with each other to form the complex and to detect the presence of a pAg.

With prior studies establishing the importance of BTN2A1 for cellular response to pAgs (Karunakaran et al., 2020; Rigau et al., 2020), we investigated the specific roles of the intracellular domains of BTN2A1 and BTN3A1 in pAg cellular detection response. In this study, we demonstrate that the BTN2A1 full intracellular domain is required for pAg detection. Through ITC (isothermal titration calorimetry) and BRET (bioluminescence resonance energy transfer) approaches, we show direct ligand inducible interactions between the intracellular domains of BTN3A1 and BTN2A1 that depend largely upon three amino acids in BTN2A1 between position 316 and 326 at the intersection of the BTN2A1 JM region with its B30.2 domain.

Results

BTN2A1 is essential for pAg detection in K562 cells by Vγ9Vδ2 T cells

We first sought to confirm the role of BTN2A1 in our system of Vγ9Vδ2 T cell mediated detection of POM_2-C-HMBP loaded cancer cells. We had previously used CRISPR/Cas9

gene editing to abrogate expression of BTN3A1 by replacing its start codon with a restriction site (Kilcollins et al., 2016; Nguyen et al., 2017). Here, we applied an analogous approach to deplete BTN2A1 in K562 cells (Figure 2A). The protospacer adjacent motif (PAM) sites were not predicted to function as well as BTN3A1, but nonetheless we attempted the favored outward facing PAM configuration with Cas9n nick sites separated by 45bp around the BTN2A1 start codon. K562 cells were transfected with the two guides in pX335 containing hSpCas9n (D10A) and a repair template. Individual clones were isolated by limiting dilution. We screened approximately 50 of the resulting clonal lines by PCR and restriction digest. We found two clones, identified as clones 1 and 27, in which the PCR product from BTN2A1 genomic template was completely cut by XhoI (Figure 2B). As a control, we also evaluated BTN3A1, and did not observe any unintended modification of this gene. The function of these clones in pAg presentation was assessed by ELISA following co-culture with Vγ9Vδ2 T cells. Relative to WT K562 cells, both clone 1 and clone 27 decreased stimulation of Vγ9Vδ2 T cell interferon γ production in response to pre-treatment with our synthetic pAg prodrug POM_2-C-HMBP (Figure 2C).

The BTN2A1 B30.2 domain is essential for pAg detection in K562 cells

We next attempted to rescue expression of BTN2A1 in clones 1 (not shown) and 27 (Figure 2). Expression of WT-BTN2A1 by transient transfection partially rescued the phenotype of the CRISPR mutant, which was statistically significant (Figure 2D). The construct expressed well as determined by Western Blot analysis of the myc epitope tag (Figure 2E). Initial attempts to improve the rescue proved unsuccessful, as did selection using G418. In light of other papers published during the course of these studies which more conclusively determined the requirement for BTN2A1 (Cano et al., 2021; Karunakaran et al., 2020; Rigau et al., 2020), we chose not to attempt further optimization of the rescue and moved forward with the partial rescue phenotype. We generated a BTN2A1 construct that lacks the full intracellular domain (pcDNA3.1-BTN2A1-ΔID). This construct expressed at similar levels to the WT BTN2A1 (Figure 2E). However, unlike the WT BTN2A1, the ΔID construct did not sensitize clone 27 to the T cell response to POM_2-C-HMBP (Figure 2F). Therefore, we concluded that the BTN2A1 internal domain is required for pAg detection in loaded K562 cells.

The intracellular domains of BTN2A1 and BTN3A1 co-localize in K562 cells

To evaluate the potential for cellular interactions between BTN2A1 and BTN3A1, we adapted a nano-bioluminescence resonance energy transfer (BRET) approach (Vasta et al., 2018). In this assay, light is produced by the enzymatic activity of nano-luciferase on a luciferin substrate, which can be used to excite fluorophores within 5–10 nm of the donor (Bacart et al., 2008; Pfleger and Eidne, 2006). Each protein (BTN2A1 or BTN3A1) was tagged at its C-terminus with either nano-luciferase or HaloTag protein. This resulted in a possibility of 4 combinations in which 2A1 or 3A1 could serve as either the BRET donor or acceptor (Figure 3A).

Upon transient transfection into WT K562 cells, the expression of the nano-luciferase tagged proteins could be assessed by detection of emitted light. Luciferase tagged BTN2A1 and 3A1 both expressed well (Figure 3B). Though variability among the independent

experiments precluded a statistically significant difference in expression, the two proteins consistently gave stronger luciferase signals relative to positive control of MDM2 proto-oncogene and BTN2A1 was generally higher than BTN3A1. The BRET ratios (which are internally controlled) were more consistent than the total luciferase signal (Figure 3C). The strongest BRET signal was observed when BTN3A1 was both the BRET donor and acceptor. Likewise, a strong signal was observed when BTN2A1 was both the donor and acceptor. Both of these homo-BRET signals were above those from the positive control pair of MDM2 and tumor protein p53 (Mazars and Fahraeus, 2010). Our BRET ratios for the positive control pair were typically lower than reported by the manufacturer. This is likely due to differences in detection method, as our instrumentation contains a 615 nm dichroic filter which results in a narrower emission bandwidth for detection of the BRET signal. The finding of strong homo-BRET readings within both BTN2A1 and BTN3A1 are consistent with prior literature suggesting these proteins each form homo-dimers.

Hetero-BRET signals were also observed which demonstrate proximity between the intracellular domains of BTN2A1 and BTN3A1 (Figure 3C). A stronger BRET signal was observed when BTN3A1 functioned as the donor and BTN2A1 as the acceptor, while a weaker BRET signal was observed when BTN2A1 was the donor and BTN3A1 the acceptor, though this weaker signal was still similar to the positive control pair. Together, this indicates that the BTN2A1 and BTN3A1 C-terminal domains are within 5–10 nm of each other under baseline or unstimulated conditions, and there may be a favored orientation or positioning.

We next evaluated whether any of the BRET signals would be impacted by pAg treatment (Figure 3D-G). Evaluation of the 4 combinations indicated that the hetero-BRET pairs, but not either of the homo-BRET pairs, were susceptible to change with pAg exposure. Addition of either 1 μM POM_2-C-HMBP or 10 μM HMBPP significantly increased the hetero-BRET signal relative to control cells in both hetero-BRET pairs. Although 10-fold less POM_2-C-HMBP was used relative to HMBPP, this synthetic pAg more potently increased the BRET signal, likely due to stability of the phosphonate substructure relative to the diphosphate. These findings are consistent in scale with a recent paper that demonstrated inducible FRET signals between the two proteins in response to treatment with the indirect pAg zoledronate (Cano et al., 2021). Together, these findings suggest that pAgs increase the proximity between the intracellular domains of the two proteins, but do not impact the proximity of the individual protein dimers.

BTN2A1 directly interacts with HMBPP-bound BTN3A1 in the intracellular domains

We performed ITC studies to probe possible direct binding between BTN3A1 and BTN2A1 in the presence or absence of HMBPP (Figure 4, Table 1). In these experiments, we used the BTN3A1 BFI construct (Hsiao et al., 2014) and a BTN2A1 construct containing its full intracellular domain (K271-L527). To reduce confusion with the 3A1 constructs, we refer to the BTN2A1 internal domain construct as ID271. The ITC results show that there is no or little heat differences when comparing the titration of ID271 into BFI and the titration of ID271 into HMBPP to the control titration. This suggests that there is no interaction between ID271 and HMBPP or BFI individually. However, once BTN3A1 BFI was preincubated

with HMBPP, there was a noticeable heat difference when BTN2A1 ID271 was titrated in. Thus, we are able to assert that the BFI:HMBPP complex has to be formed first in order to create a binding interface for ID271. The enthalpy of binding (ΔH) and entropy of binding (ΔS) was determined to be −34.94 kJ/mol and −1.20 J/mol*K, respectively (Table 1). The stoichiometry, n, was calculated to be 0.742 on average. The dissociation constant (K_d) was 0.886 μM. To further evaluate this direct interaction, we used NMR titration experiments. Unlabeled ID271 was titrated into ^{15}N-labeled BFI, as reflected in ^{15}N-HSQC spectra (Figure S1) showing concentration-dependent line-broadening throughout the entire BFI domain. Though we were unable to calculate the binding affinity from this titration data, the kinetics show that the binding is in the intermediate to slow exchange regime, so binding is likely to be at low μM range or stronger.

Mutations at the BTN2A1 JM/B30.2 intersection reduce pAg response

Prior crystallography studies have suggested that the BTN3A1 B30.2 domain may undergo dimerization, in either a putative non-symmetrical (dimer I) involving the BTN3A1 ligand binding site or a symmetrical (dimer II) opposite of the ligand binding site (Gu et al., 2017; Wang et al., 2019; Yang et al., 2019). Inspired by the regional mutagenesis approach that Scotet and colleagues used for analyzing BTN3A1 residues (Peigne et al., 2017), we performed a similar mutations in BTN2A1 focused on the regions homologous to those involved in BTN3A1 homo-dimerization, with mutations 1 and 2 expected to impact symmetrical (dimer II) formation and mutations 3–5 expected to impact non-symmetrical (dimer I) formation (Figure 5A). Plasmids containing WT-BTN2A1 or mutations 1–5 were transiently transfected into clone 27 K562 cells (Figure 5B). These cells were mixed with Vγ9Vδ2 T cells and interferon γ was measured by ELISA (Figure 5C). The results clearly demonstrated that BTN2A1 mutations 1 and 2 disrupted the pAg response while mutations 3 and 5 did not. Mutation 4 exhibited a partial phenotype, but we could not exclude weak expression of this construct relative to the others as the cause of this phenotype.

To further assess the impact of mutations 1 and 2 in BTN2A1, we generated these mutations on the pNLF-BTN2A1 plasmid for use in the BRET assays in combination with HTC-tagged BTN3A1. The mutations did not affect the total expression relative to the WT protein as determined by total luciferase units (Figure 5D). Interestingly, both mutants increased BRET between BTN2A1 and BTN3A1 in the absence of ligand (Figure 5E). At the same time, mutant 1 could be further increased by addition of ligand while mutant 2 could not. As these results may vary depending on transfection efficiency, we also normalized the data within each mutation. When normalized, both mutations did reduce the ability of POM_2-C-HMBP to promote domain proximity to BTN3A1, with mutation 2 having a slightly stronger impact in this assay (Figure 5F) which was consistent in both analyses. Additional studies showed that isolated mutations 1–5 gave similar CD spectra to WT protein (Figure S2) while mutations 1 and 2 displayed similar DSC heat curves as WT protein (Figure S3), supporting the notion that the lack of activity of mutations 1 and 2 was not due to gross protein misfolding. Together, this shows that aa316–326 within BTN2A1 are required for its function and for increasing domain proximity with BTN3A1.

Removal of the BTN2A1 JM region abrogates binding to the BTN3A1:HMBPP complex

The role of the JM region of BTN3A1 was examined through ITC as a potential mode of interaction may be through the JM helices of BTN3A1 and BTN2A1. The B30.2 domain of BTN3A1 was titrated with ID271. Similarly to BTN3A1 BFI, there is no perceptible interaction without HMBPP present (Figure 4C). Interestingly, we found that there is a strong interaction between BTN3A1 B30.2:HMBPP and BTN2A1 ID271 (Figure 4D) that is very similar to BTN3A1 BFI:HMBPP and BTN2A1 ID271 (4E). The removal of the JM region of BTN3A1 does not have any significant negative effect on the binding interaction with BTN2A1, indicating that the binding interface is located within the B30.2 of BTN3A1.

To investigate the impact of the BTN2A1 JM region on direct binding of BTN2A1 to the BTN3A1:HMBPP complex, we performed additional ITC studies using ID309 and ID328 constructs (Figure 4F,G). The ID328 construct represents the BTN2A1 B30.2 domain with no JM region (V328-L527). The ID309 construct contains a partial JM region, where the starting residue was chosen based on the sequence alignment with BTN3A1 (Q309-L527). BTN3A1 contains eight residues upstream of this position with no homologs in BTN2A1, so it seemed like a distinct sequence variation that would be of interest to investigate. While ID271 (Figure 4E) and ID309 (Figure 4F) both bound similarly to the BTN3A1:HMBPP complex, the complete removal of the JM region (ID328) significantly altered the binding of BTN2A1 to BTN3A1 as the binding curve is no longer sigmoidal, indicating that the binding affinity is much weaker (Figure 4G, H). Though the data could not be fit with confidence, there are heat differences between the titration of ID328 into BFI:HMBPP versus the titration of ID328 into buffer. There is an interaction between ID328 and the BTN3A1:HMBPP complex, providing evidence that there are residues contained in the ID328 construct that may associate with BTN3A1:HMBPP. But given that the binding affinity is much weaker, the removal of the complete JM region confirms the cellular mutation studies which suggested the most vital residues reside within the JM region of BTN2A1.

This position of binding is further narrowed down to the C-terminal end of the JM region by our BTN2A1 ID309 construct. The ITC data shows that there is binding between ID309 and BFI:HMBPP (Figure 4F). Since the K_d, n, ΔH, and ΔS values of ID309 closely resembles those of ID271 (Table 1), this suggests that ID309 contains all the necessary residues involved in the interaction. Therefore, aa271–308 are likely less important whereas aa309–327 are key for the interaction between BTN2A1 and BTN3A1:HMBPP. Thus, the region of interest determined through ITC further validates the cellular assays that pinpoint aa316–326 to be crucial for the functionality of BTN2A1.

To further evaluate the amino acid residues within the aa316–326 region, each individual amino acid was mutated (Figure 6). Most were changed in the same way as in the regional mutations 1 and 2 (Figure 6A). Due to their smaller size, we chose to mutate the two leucine residues to glycine residues instead of the leucine to alanine changes found in the regional mutations. The 11 individual mutations were evaluated by ELISA for production of interferon γ (Figure 6B). While most individual substitutions were well tolerated, L318G, W320A, and L325G all failed to rescue the depletion of BTN2A1. Of these three critical amino acids, the first two were also found in regional mutation 1 while the last was also

found in mutation 2, implicating these 3 amino acids in the lack of function of regional mutations 1 and 2. As the possibility remained that a trafficking defect was responsible for the lack of function, we evaluated the surface expression of the inactive mutants (Figure 6C/D). As a suitable BTN2A1 antibody was not available to us, we generated a 6x-his tagged version of BTN2A1 in which the his tag was sandwiched between the signal peptide and the protein. We then re-created the regional mutations 1 and 2 along with the individual mutations L318G, W320A, and L325G on the N-terminal his tagged background. The his-tagged WT BTN2A1 and all five mutations expressed well on the surface of the clone 27 cells as detected by flow cytometry using an anti-his-tag antibody. Some minor decreases were observed which were not statistically significant. Likewise, the mean fluorescence intensity in the BTN2A1 positive cells was similar among the mutants. Taken together, BTN2A1 L318, W320, and L325 are critical to the pAg response with minimal impact on surface expression of the protein.

Discussion

In this paper, we have demonstrated that the internal domain of BTN2A1 is required for response to pAgs. In our cellular assays, BTN2A1 co-localizes with other BTN2A1 molecules, but also with BTN3A1. The co-localization between full length WT BTN2A1 and BTN3A1 is observed even under baseline non-stimulatory conditions, but can be altered in their internal domains by pAg treatment. Importantly, we observed a direct biochemical interaction between the full intracellular domains of BTN3A1 and BTN2A1 in vitro, but only in the presence of pAg. This binding event occurs predominantly within the JM region of BTN2A1, and regional mutations to BTN2A1 between aa316–326 at the junction of the JM region and the B30.2 domain clearly abrogate cellular co-localization in the BRET assays and cellular function in the ELISA assays. Amino acids L318, W320, and L325 are particularly important in this regard.

While our study was ongoing, several papers were released which also show the importance of BTN2A1 for response to pAgs (Cano et al., 2021; Karunakaran et al., 2020; Rigau et al., 2020). Our findings are consistent with these papers, in that we observed a decreased response of Vγ9Vδ2 T cells to K562 cells in which BTN2A1 was depleted by CRISPR/Cas9 gene editing. The study from Herrmann and colleagues (Karunakaran et al., 2020) clearly shows extracellular interactions between the IgV domains of BTN3A1 and BTN2A1, while our study clearly demonstrates intracellular interactions within the JM region of BTN2A1 and the B30.2 domain of BTN3A1. Likely both are occurring with a cellular context. Similar to our findings, the studies from Ulrich and Olive also found a requirement for the presence of the BTN2A1 intracellular domain (Cano et al., 2021; Rigau et al., 2020) though clearly the IgV domain interacts with the TCR.

A key unknown in the field has been how pAgs trigger activation of the HMBPP receptor. Our study sheds light on this issue by identifying a direct interaction between the intracellular domains of BTN3A1 and BTN2A1, that only occurs in the presence of a pAg such as HMBPP. We demonstrated this interaction readily by ITC and NMR, and using mutagenesis, pinpoint the interaction to the aa316–326 region of BTN2A1 and specifically L318, W320, and L325. Prior functional studies demonstrated that the analogous

region within BTN3A1 is essential for activity (Peigne et al., 2017), while crystallography studies suggest this region is involved in symmetrical homo-dimerization within BTN3A1 (Gu et al., 2017). Our study suggests that for BTN2A1, the aa316–326 region is directly involved with interaction with BTN3A1. Therefore, the possibility exists that this region is involved in both homodimerization as well as interactions between the BTN2A1 dimer and the BTN3A1 dimer. That interaction of dimers could ultimately be what triggers the pAg response. As the aa316–326 region contains 5 charged amino acid residues (2 glutamates and 3 arginines), these were prime candidates for participating in the binding event. However, as it turned out, mutations of these charged residues had no effect, whereas L318, W320, and L325 were all implicated as being critical in pAg response. Interestingly, W320 is conserved among BTN2A1, BTN2A2, BTN3A1 and BTN3A3, though to our knowledge has not be investigated in these other isoforms, other than participating in the BTN3A1 homodimer dimer II interface in a crystal structure (Gu et al., 2017). Because we saw evidence for weak interactions in the absence of the JM region, we cannot fully exclude that other portions of BTN2A1 may be involved with BTN3A1 interactions.

A study from Yang used a chemical probe approach to demonstrate the importance of non-symmetric BTN3A1 dimer formation (Yang et al., 2019). Our findings do not necessarily contradict this study. In fact, because our ITC data suggests an average 1.5:1 ratio of 3A1:2A1 binding, it is possible that BTN3A1 can interact with BTN2A1 through two different modes, either as a non-symmetric dimer to monomer, or as two symmetric dimers (from our BRET data we assume that both homodimers can be formed at rest). In the former case, BTN3A1 non-symmetrical homo-dimer interacts with BTN2A1 distant JM region of aa316–326 through B30.2 domain in which HMBPP is not part of homo-dimer interface. For the later mode, the crystallography study from Gu (Gu et al., 2017) suggests that the homologous tryptophan in BTN3A1 (labelled as W284 in that paper) is involved in symmetrical homodimers of BTN3A1. Now that we know this tryptophan at the same position in BTN2A1 is critical for pAg activity, this might suggest a role for a symmetrical heterodimer between BTN2A1, formed on the L318 and L325 side of the helix, with BTN3A1 tryptophan being replaced from its interface with B30.2 domain by the BTN2A1 W320. Similarly, Wang described the corresponding region of BTN3A1 as being a critical interaction/hinge region, though did not investigate the homologous tryptophan in BTN3A1 dimer formation, rather that tryptophan was 18aa downstream (Wang and Morita, 2015; Wang et al., 2019). Thus, we believe the interaction/hinge region is not just important for BTN3A1 symmetrical homodimer formation as described by Gu and Wang, but it is also important for the interaction of BTN2A1 with BTN3A1 as our data has shown.

As a result of this study, we believe our data best fits a model where BTN2A1 and BTN3A1 dimers interact with each other to form a tetramer or similar clustered complex, which exists under baseline conditions but is increased/stabilized by pAg exposure. A study from Herrmann's group shows extracellular interactions at the IgV domains independent of pAg stimulation (Karunakaran et al., 2020). A prior study from Olive (Cano et al., 2021) demonstrated by FRET a pAg induced co-localization between BTN2A1 and BTN3A1. Our findings support both of these studies, as we also see pAg-independent homo-BRET interactions and pAg-inducible hetero-BRET interaction. In fact, the magnitude of their zoledronate induced interaction is quite similar to the magnitude of our POM_2-C-HMBP

induced interaction (both about a 3-fold increase). However, we have reached a slightly different interpretation of these results. In our study, all of the BRET interactions were observable under resting conditions. Thus, both proteins are in close proximity to each other without stimulation. Importantly, we did not observe any change in homo-BRET for BTN2A1 or BTN3A1 following pAg treatment. This suggests to us that both BTN3 and BTN2A1 each form homodimers, and pAg binding does not disrupt the homodimeric structure of either protein. We observed hetero-BRET signals between BTN3A1 and BTN2A1 in the absence of pAg, indicating that there is at least some baseline interaction between these two dimers. Yet, we see significant increases in hetero-BRET upon pAg treatment, suggesting pAgs can strengthen the interaction of the dimers.

Taken together, our study clearly shows that the full intracellular domain of BTN2A1 is required for pAg response, because it directly interacts with the BTN3A1 B30.2 domain in the presence of pAg and in cellular assays treatment with pAg increases proximity. The intersection of the BTN2A1 JM region with the B30.2 region is at least one portion of this molecule that strongly contributes to the interaction, as mutations to that region abrogate both binding and function. Our current hypothesis is that the BTN2A1 dimer and the BTN3 dimer join together through their internal domains in the presence of pAg to form a tetrameric structure as the full HMBPP receptor complex. Future studies will more clearly resolve the finer details of this activating interaction.

Limitations

One limitation of our study is that we were unable to fully optimize the re-expression of BTN2A1, leading to a partial but statistically significant rescue phenotype. The flow cytometry results in Figure 6 suggest that the transfection efficiency of our electroporation approach was around 50–60% and this likely contributed to the partial rescue in the functional studies. We cannot completely rule out that our gene editing approach affected another gene in addition to BTN2A1. Alternatively, it is possible that the transfected BTN2A1 was too highly expressed relative to endogenous and disrupted the natural stoichiometry that underlies the BTN3:BTN2A1 interaction. Indeed, our prior study found that endogenous BTN3A1 is lowly expressed in K562 cells (Kilcollins et al., 2016) and our flow cytometry studies here showed a high MFI among the BTN2A1 positive cells. A second limitation to the study is that we were unable to identify the residues of BTN3A1 that interact with BTN2A1. We were only able to narrow down the region to the B30.2 domain. Our study was designed to specifically analyze BTN2A1 and its role in pAg response, but future studies might explore the specific amino acids of BTN3A1 that may be involved in this interaction. Finally, our current model assumes that homodimers of BTN2 and homodimers of BTN3 form a tetrameric structure upon ligand binding. A caveat to the current model is that our data cannot fully exclude the possibility of a mixed 2A1–3A1 heterodimer forming and contributing to the response, as this type of structure could also give rise to the basal 2A1–3A1 proximity that we observed.

STAR Methods

RESOURCE AVAILABILITY

Lead contact—Requests for information or reagents should be directed to the Lead Contact, Andrew J. Wiemer (andrew.wiemer@uconn.edu).

Materials availability—Plasmids generated in this study are available upon request

Data and code availability—All data reported in this paper will be shared by the lead contact upon request

This paper does not report original code

Any additional information required to reanalyze the data reported in this paper is available from the lead contact upon request

EXPERIMENTAL MODEL AND SUBJECT DETAILS

Experiments described herein used co-cultures of K562 leukemia cells and primary activated Vγ9Vδ2 T cells from healthy donors. The K562 cells were cultured in RPMI-1640 containing 1.5 g/L sodium bicarbonate, 10% fetal bovine serum, and 1% penicillin streptomycin. They were maintained between 0.1 and 0.5 × 10^6 cells per mL at 37 °C in 5% carbon dioxide. The Vγ9Vδ2 T cells were obtained by magnetic bead isolation following stimulation of human PBMCs with HMBPP. PBMCs from healthy anonymous donors were purified from buffy coat using density gradient centrifugation within 24 hours of collection. Cells were counted, frozen (in 10% DMSO, 20% FBS, 70% media) and stored in liquid nitrogen. PBMCs were thawed and resuspended at 1 × 10^6 cells/mL in T cell media (RPMI-1640, 10% heat-inactivated FBS, 1x HEPES, pyruvate, NEAA, and 2-mercaptoethanol). Cells were stimulated with 0.1 μM HMBPP in the presence of IL-2 (5 ng/mL) for 3 days and cultured for another 10–14 days after compound removal. Fresh IL-2 was added every 3 days. After 10–14 days, Vγ9Vδ2 T cells were purified by magnetic bead isolation, aliquoted, and frozen. Some donors did not expand well in response to HMBPP, only cells from pAg responsive donors were used in this study.

METHOD DETAILS

Disruption and re-expression of BTN2A1—BTN2A1 was depleted from the K562 cells using CRISPR/Cas9 gene editing. CRISPR/Cas9 was used according to the method of Cong (Cong et al., 2013) and Ran (Ran et al., 2013) as we previously modified for BTN3A1 (Kilcollins et al., 2016). sgRNAs were designed to remove a region of genomic DNA containing the BTN2A1 start codon. The sgRNAs cloned into pX335-U6-Chimeric_BB-CBh-hSpCas9n (D10A) were: 5’ - CAC CGC TGC TGC CCT GCA CTT CTC C-3’ (sense) and 5’ - CAC CGA TTC CAT GAG CAC CCA GAG C - 3’ (antisense). To facilitate homology directed repair, cells were co-transfected with a 192-bp single stranded repair template: (5’- GAG TGA CGG GAG AGG TTG GGC CCG ACC AGC ACT GAG GTG CCA AGA CTC CTA GGC TGA TTC TCC TCT GTA ACC CTA GGC CTC CTG TCC CTG CCT CCC TCG AGG ATA TCC CCG GCC AGC CTC CCT CCT CCT CCT CCT

CCT CAG CCT GTG TGC ACT GGT CTC AGG TAG GGA TGT GTG CCA CTT GCT GCT GTC ACC - 3'). The repair template contained central restriction sites for XhoI and EcoRV to facilitate genotyping. Transfection was performed by electroporation with a gene pulser XCELL (Biorad) using the exponential protocol set at 316 volts, 500 μF capacitance and 4 mm conditions. The transfection was performed using 1×10^7 cells, 10 μg of each sgDNA plasmid, and 200 pg ssODN in 400 μL volume. At 24 hours post-transfection, single cells were separated by limiting dilution and allowed to grow as clonal colonies for 3–4 weeks.

To identify the mutated clones, genomic DNA from individual clones was isolated by re-suspension of the cells from 1 mL culture in buffer (8 mM Tris, 5 mM EDTA, 200 mM NaCl, 0.2% SDS pH 8.0) containing 200 μg/mL proteinase K (Fisher) followed by heating at 55 °C for 1 hour, isopropanol precipitation, 70% ethanol wash, and re-suspension in water. Genotyping of BTN2A1 was performed by PCR of genomic DNA with the following primers: 5' - ATC CCT CTC TCG GGA CAT AC - 3' and 5' - CAA CTC CAC AGT CCT TCT TTC T - 3'. Genotyping of BTN3A1 was performed as described as a control (Kilcollins et al., 2016). The mutant DNA was assessed by test digest of the PCR amplicons with XhoI.

In BTN2A1 deficient cells, BTN2A1 was re-introduced by transient transfection. BTN2A1 was cloned into pcDNA3.1 (+) using the following primers: forward primer into NheI site 5' - GCT ATC GCT AGC ATG GAA TCA GCT GCT GCC CT - 3', reverse primer into XhoI site including myc tag and stop codon 5' - GCT ATC CTC GAG CTA CAG ATC CTC TTC TGA GAT GAG TTT TTG TTC TAG GCT CTG GTG GGT C - 3' and validated by Sanger sequencing. BTN2A1 lacking the internal domain (ΔID) was generated from the full-length protein in pcDNA 3.1 (+) using the following primers: forward 5' - GAA CAA AAA CTC ATC TCA GAA G - 3', reverse 5' - CCC TGA CAG AAT CTT TTT TTC C - 3'. The plasmids (20 μg) were electroporated using the above conditions into $5–10 \times 10^6$ K562 cells.

The N-terminal 6x-his tagged BTN2A1 in pcDNA3.1 (+) was generated from the C-terminal myc tagged BTN2A1 in pcDNA3.1 (+). As we desired to both remove the C-terminal myc tag and insert the new his tag between the signal peptide and IgV domain, we performed two PCR reactions (one for the gene and one for the plasmid), used splicing by overlap extension (SOE) to join them, then self-circularized. For the gene amplification, we used 5' - GAG AAT TTG TAT TTT CAG GGT CAG TTT ATT GTC GTG GGG C - 3' and 5' - TAG GCT CTG GTG GGT C - 3'. For the backbone amplification we used 5' - TGA CTC GAG TCT AGA GGG C - 3' and 5' - CTG AAA ATA CAA ATT CTC CCC GGC GTG ATG ATG ATG ATG ATG ATG ACC GGC TGA GAC CAG TGC ACA - 3'. The smaller primers of each pair were phosphorylated and used for SOE. The SOE product was gel purified and self-circularized using T4 DNA ligase.

ELISA—In order to assess the activation of the Vγ9Vδ2 T cells by pAg loaded K562 cells, secreted interferon γ was quantified by ELISA. The transiently transfected K562 cells at 24 hours post transfection were suspended in fresh T cell media and treated with various doses of POM_2-C-HMBP from 0.1 nM to 1 μM for 1 hour. K562 cells were washed twice and mixed with expanded pAg-responsive Vγ9Vδ2 T cells (4,000 K562 cells and 12,000 T cells

per well) in 96 well plates. Mixtures were incubated for 20 hours, after which ELISA was performed according to the manufacturer's protocol (Biolegend). Rescue experiments with the mutants are expressed as a percentage of the clone 27+WT BTN2A1 level following stimulation with 0.1 to 1 uM of POM_2-C-HMBP as indicated.

Nano-BRET assays—The proximity of BTN2A1 and BTN3A1 internal domains in a cellular context were assessed using nano-BRET (Promega). BTN2A1 and BTN3A1 were cloned into the pHTC and the pNLF1-C vectors to attach the HaloTag and the nano-luciferase tag to each protein at its C-terminus. BTN2A1 was amplified from plasmid template by PCR using the forward primer 5'-GCT ATC GCT AGC ATG GAA TCA GCT GCT GCC C - 3' and the reverse primer 5'- GCT ATC GAG CTC CTA GGC TCT GGT GGG TC - 3' which allowed for directional insertion into pHTC and pNLF1-C using the NheI and SacI cut sites. BTN3A1 was amplified from plasmid template by PCR using the forward primer 5'- GCT ATC GCT AGC ATG AAA ATG GCA AGT TTC CT - 3' and the reverse primer 5'- GCT ATC GAG CTC CCG CTG GAC AAA TAG TCA G - 3' which also allowed for directional insertion. The four new constructs were validated by Sanger sequencing.

The vectors containing halo-tagged and nano-luciferase-tagged BTN2A1 and BTN3A1 were transfected into WT K562 cells by electroporation. Transfection was performed by electroporation using above conditions. These transfections were performed using 5×10^6 cells, 20 μg of each pHTC plasmid, and 2 μg of each pNLF1-C plasmid or as indicated in 400 μL volume of antibiotic-free media, then diluted into 5 mL of antibiotic-free media. After 20 hours, the cells were further diluted to 0.2×10^6 cells/mL in normal K562 media, the HaloTag NanoBRET 618 ligand was added to a final concentration of 100 nM, and the cells were arrayed into 96 well plates (100 μL/well). Cells were treated as indicated in the text. After 24 hours, the NanoBRET NanoGlo substrate solution was added at 1:1000 dilution, and the luminescence was detected within 15 minutes using a Perkin Elmer VICTOR X5. Measurements were taken using no emission filter to assess total luminescence and a 615 nm dichroic filter to assess BRET signal. A BRET/total signal ratio was calculated for each well, and background from controls that contained no 618 nm ligand was subtracted to give the final BRET values. The positive control pair of p53 and MDM2 was supplied by the manufacturer.

BTN2A1 regional mutations—Site directed mutagenesis by PCR was used to generate regional mutations of BTN2A1 in the pcDNA3.1 (+) or the pNLF1-C vectors. The primers used were as follows: mut1-F, 5' - GGA GCT GCT GGT GCT GCA AGA ACA TTC TTA CAT GCT GTT G – 3'; mut1-R, 5' - TTG AAG TTT CTC TTT TAC TTG AAG TTC - 3'; mut2-F, 5' - GGA GCT GGT GCT GCA GCT GTT GAT GTG GTC CTG - 3'; mut2-R, 5' - TCT CCA TCG CAA TTC TTC TT - 3'; mut3-F, 5' - GCT GGT GCT GCA GGA AGT GTG AGA AGG TGC C - 3'; mut3-R, 5' - CAG GAA GAG ATC GGG ATG A - 3'; mut4-F, 5' - GCT GGT GCT GCA GGA CCC TTC AGG CAC CTA GGG GA - 3'; mut4-R, 5' - TCT CCG GTC CTC TGA CAG GAA - 3'; mut5-F, 5' - GGA GCT GCT GGT GCT GCA AGC GTG CCT GAC AAC C - 3'; mut5-R, 5' - GGG GCA CCT TCT CAC A - 3'. The circular parental plasmid templates were cleared using DpnI. The

remaining PCR amplicon was phosphorylated with T4 kinase and ligated with T4 ligase before transformation. Mutations were validated by Sanger sequencing.

BTN2A1 single amino acid mutations—Site directed mutagenesis by PCR was used to generate single amino acid mutations of BTN2A1 in the pcDNA3.1 (+) vector. The following forward primers were used in combination with mut1-R listed in the prior section: E316G-F, 5’ - GGA GAA TTG CGA TGG AGA AGA ACA - 3’; E317A-F, 5’ - GAA GCT TTG CGA TGG AGA AGA ACA TT - 3’; L318G-F, 5’ - GAA GAA GGG CGA TGG AGA AGA ACA TTC TTA CAT - 3’; R319G-F, 5’ - GAA GAA TTG GGT TGG AGA AGA ACA TTC TTA CAT GC - 3’; W320A-F, 5’ - GAA GAA TTG CGA GCT AGA AGA ACA TTC TTA CAT GCT GTT - 3’; R321A-F, 5’ - GAA GAA TTG CGA TGG GCA AGA ACA TTC TTA CAT GCT GTT G - 3’. The following forward primers were used in combination with mut2-R listed in the prior section: R322G-F, 5’ - GGA ACA TTC TTA CAT GCT GTT GAT - 3’; T323A-F, 5’ - AGA GCT TTC TTA CAT GCT GTT GAT GTG - 3’; F324G-F, 5’ - AGA ACA GGT TTA CAT GCT GTT GAT GTG GT - 3’; L325G-F, 5’ - AGA ACA TTC GGA CAT GCT GTT GAT GTG GTC CT - 3’; H326A-F, 5’ - AGA ACA TTC TTA GCA GCT GTT GAT GTG GTC CTG - 3’. The circular parental plasmid templates were cleared using DpnI. The remaining PCR amplicon was phosphorylated with T4 kinase and ligated with T4 ligase before transformation. Mutations were validated by Sanger sequencing.

Protein expression and purification—The butyrophilin constructs for use in biochemical assays were obtained by directional cloning. Recombinant BTN3A1 BFI (*h*BTN3A1$^{272-513}$), the full intracellular domain of human BTN3A1 containing both the juxtamembrane (JM) and B30.2 domain, as well as a construct containing only the BTN3A1 B30.2 domain (*h*BTN3A1$^{340-513}$), were previously cloned into pET21b vector as described (Hsiao et al., 2014). Recombinant BTN2A1 ID271 (*h*BTN2A1$^{271-527}$), the full intracellular domain of human BTN2A1, was cloned into the pET21b NdeI/XhoI sites by a similar approach using the forward primer 5’- GCT ATC CAT ATG AAA CTC CAA AAG GAA AAA AAG ATT - 3’ and the reverse primer 5’- GCT ATC CTC GAG TAG GCT CTG GTG GGT C - 3’. The shorter constructs ID309 (*h*BTN2A1$^{309-527}$) and ID328 (*h*BTN2A1$^{328-527}$) were generated with the same reverse primer as above and the following forward primers: ID309, 5’ - GCT ATC CAT ATG CAA GTA AAA GAG AAA CTT CAA GA - 3’; ID328, 5’ - GCT ATC CAT ATG GTT GAT GTG GTC CTG GAT C - 3’. The plasmids were purified from *Escherchia coli* DH5α cells, validated by Sanger sequencing and re-transformed into *E. coli* Rosetta 2 (DE3) pLysS cells for protein expression.

The proteins were expressed and purified from bacterial cultures. From a single colony, bacterial cultures were grown overnight in LB media containing ampicillin and chloramphenicol at 37°C to be transferred to LB or M9 minimal media. For M9 minimal media, $^{15}NH_4Cl$ was added as the sole nitrogen source. Bacterial cultures were grown at 37°C until the OD_{600} was approximately 0.5. The cells were transferred to room temperature and allowed to equilibrate for an hour. The cells were induced by treatment with 1 mM isopropyl β-d-1-thiogalactopyranoside (IPTG) for overnight induction (~18 hours) at room temperature before harvesting. Purification of the recombinant proteins was initiated by lysing cells with three passages through a French Press homogenizer (Thermo Fisher

Scientific) in lysis buffer (50 mM Tris, 200 mM NaCl, 10 mM 2-mercaptoethanol, and 5 mM imidazole, pH 7.4). The cell lysate was centrifuged at 8000 rpm for one hour at 4 °C. The supernatant was mixed with NiNTA agarose resin (Qiagen) for 45 minutes at 4 °C. The resin was washed (50 mM Tris, 200 mM NaCl, 10 mM 2-mercaptoethanol, and 20 mM imidazole, pH 7.4) prior to eluting the protein (50 mM Tris, 200 mM NaCl, 10 mM 2-mercaptoethanol, and 300 mM imidazole, pH 7.4). The elution was loaded onto a Superdex 75 16/600 HiLoad Column (GE Healthcare), equilibrated with 50 mM Tris, 100 mM NaCl, and 5 mM 2-mercaptoethanol, pH 7.5, to obtain the final purified protein for subsequent experiments.

Isothermal Titration Calorimetry—ITC was conducted using a low volume nanoITC (TA instruments). The buffer was 50 mM tris, 100 mM NaCl, and 5 mM 2-mercaptoethanol at pH 7.5. The experimental parameters were 25 °C, 20 injections, 2.5 μL per injection, 300 s injection interval, and 200 rpm for stirring. The concentration of the titrant varied from 300 μM to 400 μM whereas the titrand was from 40 μM to 80 μM. For titrations with both BFI and HMBPP present, the ratio of BFI:HMBPP was 1:2. The data was analyzed using NanoAnalyze (TA instruments) with the independent fit model.

Nuclear Magnetic Resonance—Interactions between BTN3A1 and BTN2A1 were confirmed through ^{1}H-^{15}N HSQC experiments performed on a Varian Inova 600-MHz spectrometer (Agilent Technologies) at 25°C. Spectra were collected using 1024 · 128 increments. The buffer contained 50 mM tris, 100 mM NaCl, 5 mM 2-mercaptoethanol, and 8% D_2O at pH 7.5. Titration of ^{15}N BFI and HMBPP at a 1:2 molar ratio with ID271 was performed, where the molar ratio of ID271:BFI was 0.25:1, 0.5:1, and 1:1. Processing and analysis of NMR data was done using NMRPipe and CcpNmr, provided by the NMRbox server (Delaglio et al., 1995; Maciejewski et al., 2017; Vranken et al., 2005).

Differential Scanning Calorimetry—Protein unfolding temperatures were measured with a NanoDSC (TA instruments). Heating curves were collected from 10 °C to 120 °C at a heating rate of 1 °C per minute. The pressure was held constant at 3 atm. Samples were in a buffer of 50 mM tris, 100 mM NaCl, and 5 mM 2-mercaptoethanol at pH 7.5. The protein concentration used was 100 μM. The data was analyzed using NanoAnalyze (TA instruments) with two state scaled fit model.

Circular Dichroism—CD was performed using Chirascan V100 (Applied Photophysics) with a 1mm Spectrosil quartz cuvette (Starna Cells). Data was collected at 20°C at a spectral range of 200nm to 260nm with 1 nm bandwidth, 1 nm step size, and 5 seconds per step. Protein concentrations were 3 μM and were in a buffer consisting of 10 mM K_3PO_4 and 50 mM Na_2SO_4 at pH 7.5.

BTN2A1 Surface Expression—Clone 27 was transiently transfected with pcDNA3.1 (+) containing BTN2A1 with the extracellular his tag in the WT or mutated form. At 24 hours, ~1 million cells were resuspended in FACS buffer (2% BSA in PBS) stained with 3 μL of PE anti-his tag antibody for 30 minutes, washed twice with FACS buffer, resuspended in FACS buffer, and fixed with 3% paraformaldehyde. Cells were gated with FSC and SSC for the

major K562 cell population, then percent of PE positive cells and their mean fluorescence intensity were determined.

QUANTIFICATION AND STATISTICAL ANALYSIS

The number of independent experiments (n) is listed for each figure. ANOVA was used to calculate significance in bar graphs as indicated. Comparisons were done relative to the control or between pairs of conditions. Columns in bar graphs represent the mean ± SEM or STDEV as indicated in the figure legends. An α level of 0.05 or 0.01 was used as indicated. Dose response curves were analyzed using non-linear regression (log [agonist] versus response) in GraphPad Prism.

Supplementary Material

Refer to Web version on PubMed Central for supplementary material.

Acknowledgments

Financial support from the NIH (AI150869 to AJW and OV) is gratefully acknowledged.

References

Bacart J, Corbel C, Jockers R, Bach S, and Couturier C (2008). The BRET technology and its application to screening assays. Biotechnol J 3, 311–324. [PubMed: 18228541]

Cano CE, Pasero C, De Gassart A, Kerneur C, Gabriac M, Fullana M, Granarolo E, Hoet R, Scotet E, Rafia C, et al. (2021). BTN2A1, an immune checkpoint targeting Vγ9Vδ2 T cell cytotoxicity against malignant cells. Cell Rep 36, 109359. [PubMed: 34260935]

Cong L, Ran FA, Cox D, Lin S, Barretto R, Habib N, Hsu PD, Wu X, Jiang W, Marraffini LA, et al. (2013). Multiplex genome engineering using CRISPR/Cas systems. Science 339, 819–823. [PubMed: 23287718]

Delaglio F, Grzesiek S, Vuister GW, Zhu G, Pfeifer J, and Bax A (1995). NMRPipe: a multidimensional spectral processing system based on UNIX pipes. J Biomol NMR 6, 277–293. [PubMed: 8520220]

Gu S, Borowska MT, Boughter CT, and Adams EJ (2018). Butyrophilin3A proteins and Vγ9Vδ2 T cell activation. Semin Cell Dev Biol 84, 65–74. [PubMed: 29471037]

Gu S, Sachleben JR, Boughter CT, Nawrocka WI, Borowska MT, Tarrasch JT, Skiniotis G, Roux B, and Adams EJ (2017). Phosphoantigen-induced conformational change of butyrophilin 3A1 (BTN3A1) and its implication on Vγ9Vδ2 T cell activation. Proc Natl Acad Sci U S A 114, E7311–E7320. [PubMed: 28807997]

Harly C, Guillaume Y, Nedellec S, Peigne CM, Monkkonen H, Monkkonen J, Li J, Kuball J, Adams EJ, Netzer S, et al. (2012). Key implication of CD277/butyrophilin-3 (BTN3A) in cellular stress sensing by a major human γδ T-cell subset. Blood 120, 2269–2279. [PubMed: 22767497]

Hsiao CC, and Wiemer AJ (2018). A power law function describes the time- and dose-dependency of Vγ9Vδ2 T cell activation by phosphoantigens. Biochem Pharmacol 158, 298–304. [PubMed: 30391478]

Hsiao CH, Lin X, Barney RJ, Shippy RR, Li J, Vinogradova O, Wiemer DF, and Wiemer AJ (2014). Synthesis of a phosphoantigen prodrug that potently activates Vγ9Vδ2 T-lymphocytes. Chem Biol 21, 945–954. [PubMed: 25065532]

Karunakaran MM, Willcox CR, Salim M, Paletta D, Fichtner AS, Noll A, Starick L, Nohren A, Begley CR, Berwick KA, et al. (2020). Butyrophilin-2A1 Directly Binds Germline-Encoded Regions of the Vγ9Vδ2 TCR and Is Essential for Phosphoantigen Sensing. Immunity 52, 487–498. [PubMed: 32155411]

Kilcollins AM, Li J, Hsiao CH, and Wiemer AJ (2016). HMBPP Analog Prodrugs Bypass Energy-Dependent Uptake To Promote Efficient BTN3A1-Mediated Malignant Cell Lysis by Vγ9Vδ2 T Lymphocyte Effectors. J Immunol 197, 419–428. [PubMed: 27271567]

Laplagne C, Ligat L, Foote J, Lopez F, Fournie JJ, Laurent C, Valitutti S, and Poupot M (2021). Self-activation of Vγ9Vδ2 T cells by exogenous phosphoantigens involves TCR and butyrophilins. Cell Mol Immunol 18, 1861–1870. [PubMed: 34183807]

Maciejewski MW, Schuyler AD, Gryk MR, Moraru II, Romero PR, Ulrich EL, Eghbalnia HR, Livny M, Delaglio F, and Hoch JC (2017). NMRbox: A Resource for Biomolecular NMR Computation. Biophys J 112, 1529–1534. [PubMed: 28445744]

Mazars A, and Fahraeus R (2010). Using BRET to study chemical compound-induced disruptions of the p53-HDM2 interactions in live cells. Biotechnol J 5, 377–384. [PubMed: 20235143]

McCarthy NE, and Eberl M (2018). Human γδ T-Cell Control of Mucosal Immunity and Inflammation. Front Immunol 9, 985. [PubMed: 29867962]

Morita CT, Jin C, Sarikonda G, and Wang H (2007). Nonpeptide antigens, presentation mechanisms, and immunological memory of human Vγ9Vδ2 T cells: discriminating friend from foe through the recognition of prenyl pyrophosphate antigens. Immunol Rev 215, 59–76. [PubMed: 17291279]

Nguyen K, Li J, Puthenveetil R, Lin X, Poe MM, Hsiao CC, Vinogradova O, and Wiemer AJ (2017). The butyrophilin 3A1 intracellular domain undergoes a conformational change involving the juxtamembrane region. FASEB J 31, 4697–4706. [PubMed: 28705810]

Payne KK, Mine JA, Biswas S, Chaurio RA, Perales-Puchalt A, Anadon CM, Costich TL, Harro CM, Walrath J, Ming Q, et al. (2020). BTN3A1 governs antitumor responses by coordinating αβ and γδ T cells. Science 369, 942–949. [PubMed: 32820120]

Peigne CM, Leger A, Gesnel MC, Konczak F, Olive D, Bonneville M, Breathnach R, and Scotet E (2017). The Juxtamembrane Domain of Butyrophilin BTN3A1 Controls Phosphoantigen-Mediated Activation of Human Vγ9Vδ2 T Cells. J Immunol 198, 4228–4234. [PubMed: 28461569]

Pfleger KD, and Eidne KA (2006). Illuminating insights into protein-protein interactions using bioluminescence resonance energy transfer (BRET). Nat Methods 3, 165–174. [PubMed: 16489332]

Poe MM, Agabiti SS, Liu C, Li V, Teske KA, Hsiao CC, and Wiemer AJ (2019). Probing the Ligand-Binding Pocket of BTN3A1. J Med Chem 62, 6814–6823. [PubMed: 31268699]

Ran FA, Hsu PD, Wright J, Agarwala V, Scott DA, and Zhang F (2013). Genome engineering using the CRISPR-Cas9 system. Nat Protoc 8, 2281–2308. [PubMed: 24157548]

Riano F, Karunakaran MM, Starick L, Li J, Scholz CJ, Kunzmann V, Olive D, Amslinger S, and Herrmann T (2014). Vγ9Vδ2 TCR-activation by phosphorylated antigens requires butyrophilin 3 A1 (BTN3A1) and additional genes on human chromosome 6. Eur J Immunol 44, 2571–2576. [PubMed: 24890657]

Rigau M, Ostrouska S, Fulford TS, Johnson DN, Woods K, Ruan Z, McWilliam HEG, Hudson C, Tutuka C, Wheatley AK, et al. (2020). Butyrophilin 2A1 is essential for phosphoantigen reactivity by γδ T cells. Science 367, eaay5516. [PubMed: 31919129]

Sandstrom A, Peigne CM, Leger A, Crooks JE, Konczak F, Gesnel MC, Breathnach R, Bonneville M, Scotet E, and Adams EJ (2014). The intracellular B30.2 domain of butyrophilin 3A1 binds phosphoantigens to mediate activation of human Vγ9Vδ2 T cells. Immunity 40, 490–500. [PubMed: 24703779]

Vantourout P, and Hayday A (2013). Six-of-the-best: unique contributions of γδ T cells to immunology. Nat Rev Immunol 13, 88–100. [PubMed: 23348415]

Vasta JD, Corona CR, Wilkinson J, Zimprich CA, Hartnett JR, Ingold MR, Zimmerman K, Machleidt T, Kirkland TA, Huwiler KG, et al. (2018). Quantitative, Wide-Spectrum Kinase Profiling in Live Cells for Assessing the Effect of Cellular ATP on Target Engagement. Cell Chem Biol 25, 206–214. [PubMed: 29174542]

Vermijlen D, Gatti D, Kouzeli A, Rus T, and Eberl M (2018). γδ T cell responses: How many ligands will it take till we know? Semin Cell Dev Biol 84, 75–86. [PubMed: 29402644]

Vranken WF, Boucher W, Stevens TJ, Fogh RH, Pajon A, Llinas M, Ulrich EL, Markley JL, Ionides J, and Laue ED (2005). The CCPN data model for NMR spectroscopy: development of a software pipeline. Proteins 59, 687–696. [PubMed: 15815974]

Wang H, and Morita CT (2015). Sensor Function for Butyrophilin 3A1 in Prenyl Pyrophosphate Stimulation of Human Vγ9Vδ2 T Cells. J Immunol 195, 4583–4594. [PubMed: 26475929]

Wang H, Nada MH, Tanaka Y, Sakuraba S, and Morita CT (2019). Critical Roles for Coiled-Coil Dimers of Butyrophilin 3A1 in the Sensing of Prenyl Pyrophosphates by Human Vγ9Vδ2 T Cells. J Immunol 203, 607–626. [PubMed: 31227581]

Wiemer AJ (2020). Structure-Activity Relationships of Butyrophilin 3 Ligands. ChemMedChem 15, 1030–1039. [PubMed: 32453919]

Willcox BE, and Willcox CR (2019). γδ TCR ligands: the quest to solve a 500-million-year-old mystery. Nat Immunol 20, 121–128. [PubMed: 30664765]

Yang Y, Li L, Yuan L, Zhou X, Duan J, Xiao H, Cai N, Han S, Ma X, Liu W, et al. (2019). A Structural Change in Butyrophilin upon Phosphoantigen Binding Underlies Phosphoantigen-Mediated Vγ9Vδ2 T Cell Activation. Immunity 50, 1043–1053. [PubMed: 30902636]

Significance

Traditional models of T cell activation describe presentation of peptide antigens by MHC for detection by the T cell receptor. However, many non-traditional T cells have now been identified, including γδ T cells. The mechanisms of antigen detection by non-traditional T cells are not well-understood, but it is clear that the traditional models do not fully apply. It has been known for decades that the Vγ9Vδ2 subset detects pAgs, but only recently have studies identified butyrophilin (BTN) proteins as partners in this process. To shed light on the interactions between BTN3A1 and BTN2A1 we used three complementary approaches (ITC, nano-BRET, and ELISA) to assess how pAg binding affects the structure and function of these proteins. We demonstrate that pAgs promote binding between the purified internal domains of these proteins. These interactions also occur in cells, and are necessary for detection of the pAg receptor complex by the Vγ9Vδ2 TCR. The interaction involves the JM region of BTN2A1 interacting with the B30.2 domain of BTN3A1, and mutations to specific amino acid residues (L318, W320, and L325) in BTN2A1 can abrogate this response. Our data is consistent with a model of the BTN2A1 dimer and the BTN3A1 dimer join together through their internal domains in the presence of pAg to form a tetrameric structure as the full HMBPP receptor complex. These findings have implications for the understanding of non-traditional T cell antigen detection.

Highlights

- The BTN2A1 internal domain is required for Vγ9Vδ2 T cell phosphoantigen response
- The BTN2A1 internal domain binds to BTN3A1 in the presence of phosphoantigen
- The JM region of BTN2A1, but not of BTN3A1, is required for their interaction
- Mutations to BTN2A1 L318, W320, and L325 abrogate phosphoantigen response

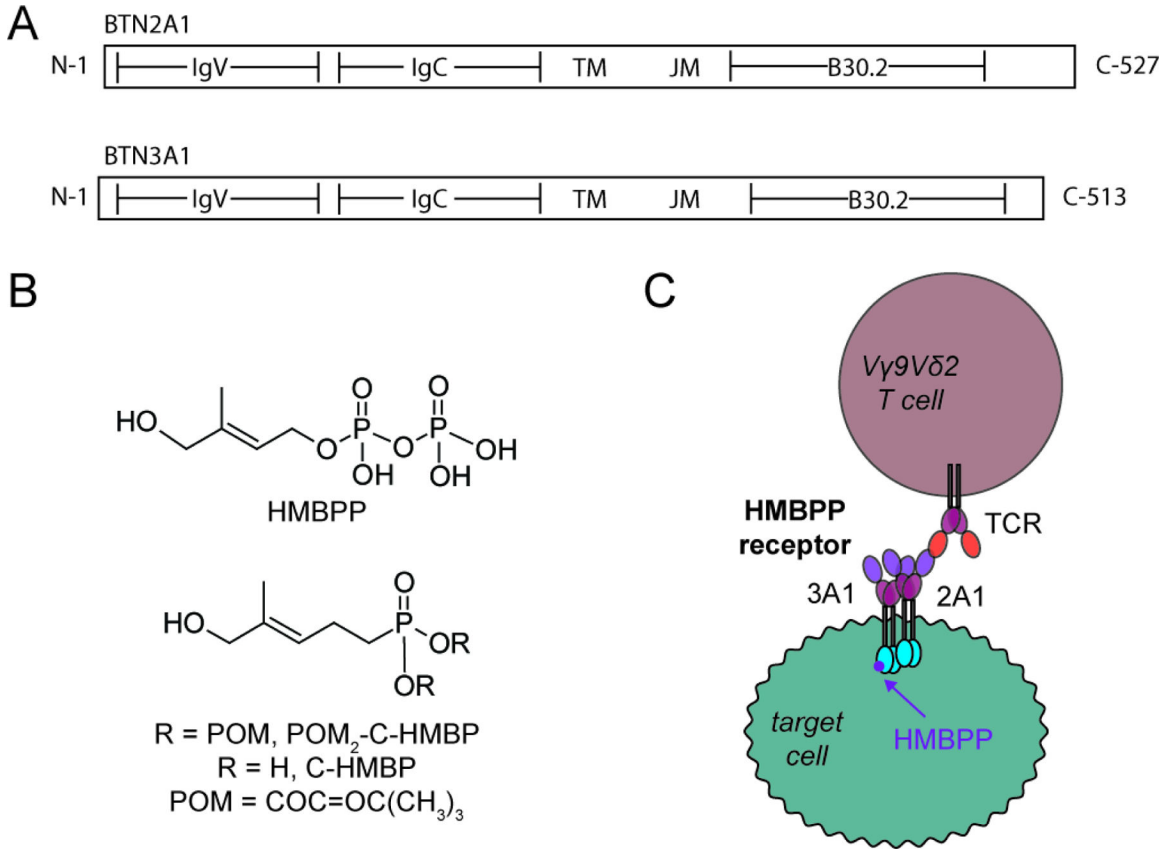

Figure 1. The HMBPP receptor.

A) BTN2A1 and BTN3A1 are single pass transmembrane proteins with extracellular immunoglobulin domains and intracellular B30.2 domains, connected by the transmembrane and JM regions. B) Chemical structures of HMBPP and its synthetic analogs POM_2-C-HMBP and C-HMBP. C) Ligands such as HMBPP bind to the B30.2 domain of BTN3A1, activating the receptor complex for detection by the γδ TCR. The current study examines the role of the BTN internal domains in this process.

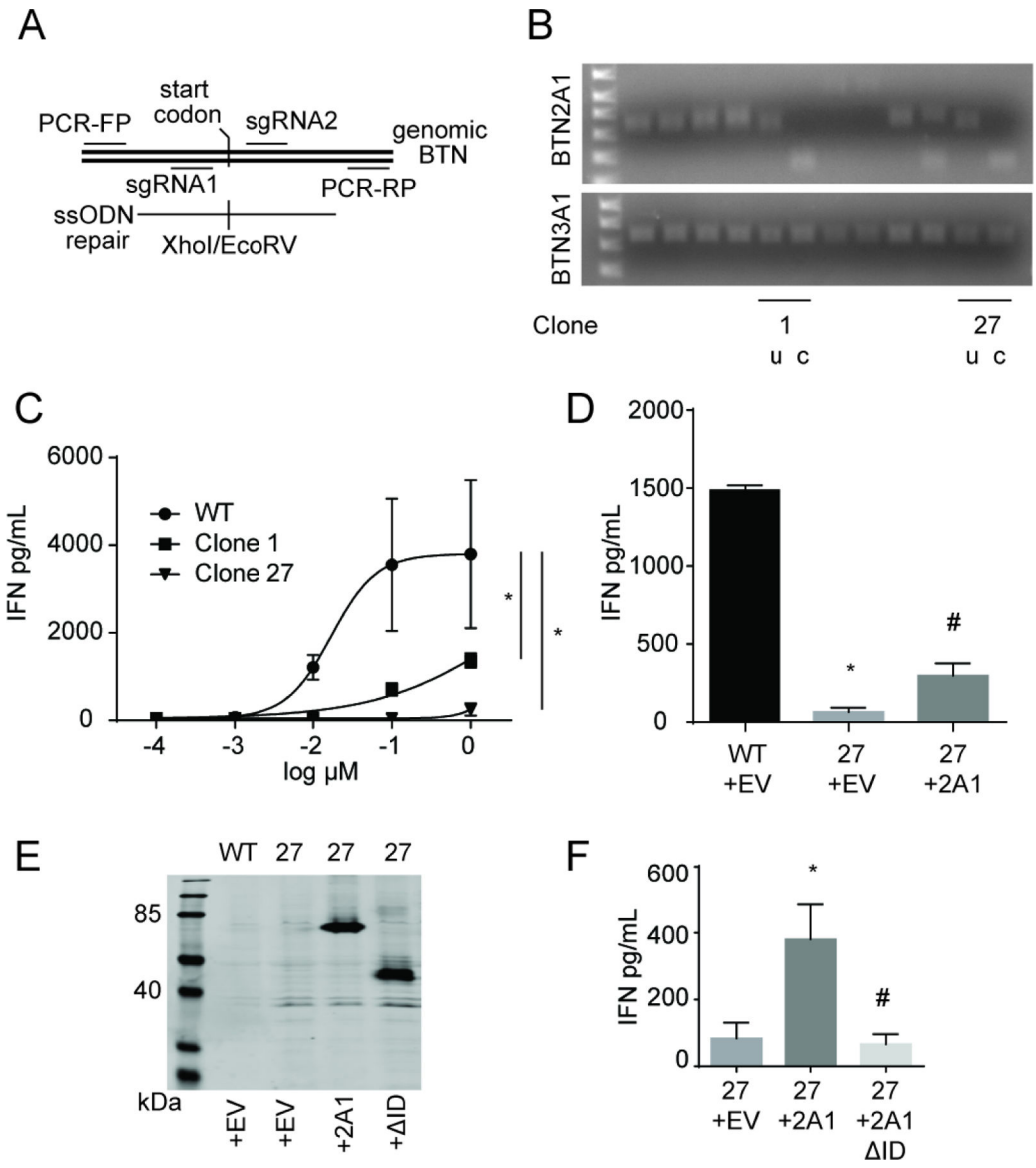

Figure 2. BTN2A1 and its internal domain are required for pAg response in K562 cells.

A) The region surrounding the start codon of BTN2A1 was removed using Crispr/Cas9n with two sgRNA guides, and replaced with a double restriction site to facilitate genotyping. B) The region of modified genomic BTN2A1 and BTN3A1 from selected K562 clones was amplified by PCR and cut with XhoI. Clones 1 and 27 are marked in their uncut (u) and cut (c) forms. Representative of n=2. C) K562 cells were treated with POM_2-C-HMBP then mixed with Vγ9Vδ2 T cells. Interferon-γ was detected by ELISA. *$p<0.05$ when comparing the curves by extra sum-of-squares F test, (n=3). D) pcDNA3.1 (+) (EV) or pcDNA3.1 (+) containing WT-BTN2A1 (2A1) were transfected into WT K562 cells (WT) or clone 27 K562 cells (27) and mixed with Vγ9Vδ2 T cells. Interferon-γ was detected by ELISA. *$p<0.05$ relative to WT+EV, $^{\#}p<0.05$ relative to 27+EV, one-way ANOVA, (n=3). E) Expression of BTN2A1 and BTN2A1ΔID by Western Blot for the myc epitope tag. Representative of n=3 replicates. F) pcDNA3.1 (+) (EV) or pcDNA3.1 (+) containing

WT-BTN2A1 (2A1) or WT-BTN2A1ΔID were transfected into clone 27 K562 cells (27) and mixed with Vγ9Vδ2 T cells. Interferon-γ was detected by ELISA. *$p<0.05$ relative to 27+EV, $^{\#}p<0.05$ relative to 27+2A1, one-way ANOVA, (n=3). Columns in bar graphs represent the mean ± SEM.

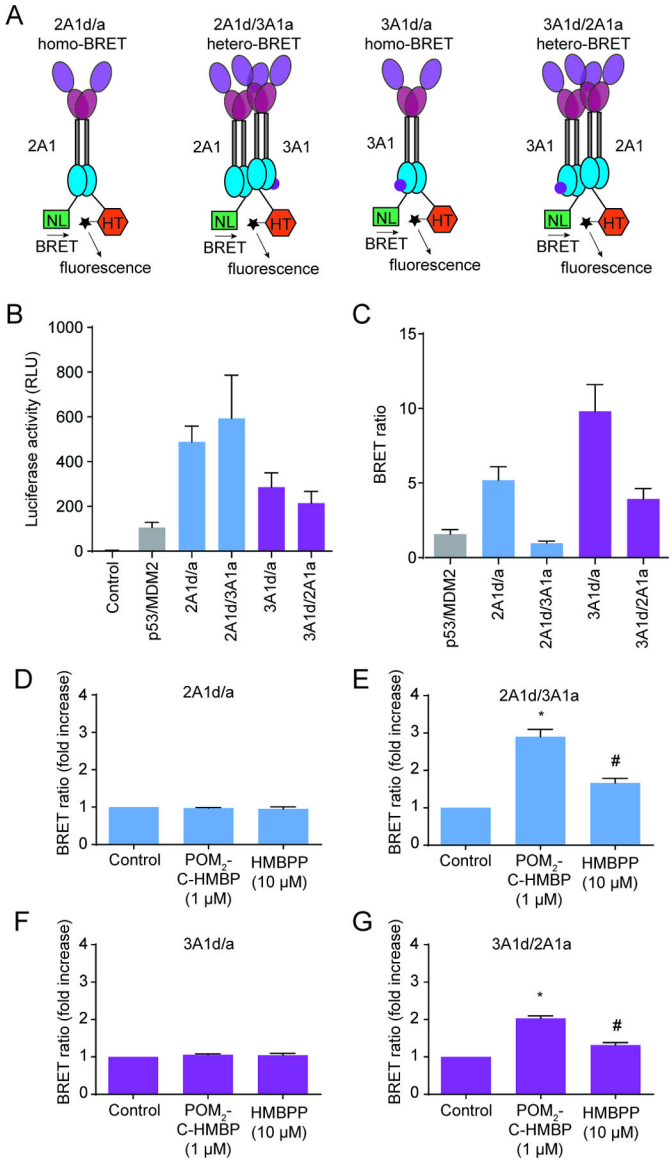

Figure 3. The internal domains of BTN2A1 and BTN3A1 are co-localized with pAg-dependent signals detected by nano-BRET.

A) Nano BRET tags were applied to the C terminus of BTN2A1 and BTN3A1 in varying donor (d) or acceptor (a) combinations. This enabled detection of co-localization between two molecules of the same protein (homo-BRET) or two molecules of different proteins (hetero-BRET). BRET occurs between the nano-luciferase (NL) from the donor and the 618 nm HaloTag ligand (star) bound to the HaloTag (HT) on the acceptor. B) Luciferase readings from K562 cells transiently transfected with varying combinations of the BRET probes (n=6). C) BRET ratios for varying combinations of the BTN BRET probes relative to the p53/MDM2 positive control (n=3). D-G) BRET ratios for K562 cells transfected with indicated combinations following overnight treatment with POM_2-C-HMBP (1 μM) or HMBPP (10 μM) (n=3). Statistical significance was determined by one-way ANOVA with Tukey's post-hoc analysis. *$p < 0.05$ versus corresponding control, #$p < 0.05$ versus

corresponding control and POM_2-C-HMBP treated cells. Columns in bar graphs represent the mean ± SEM.

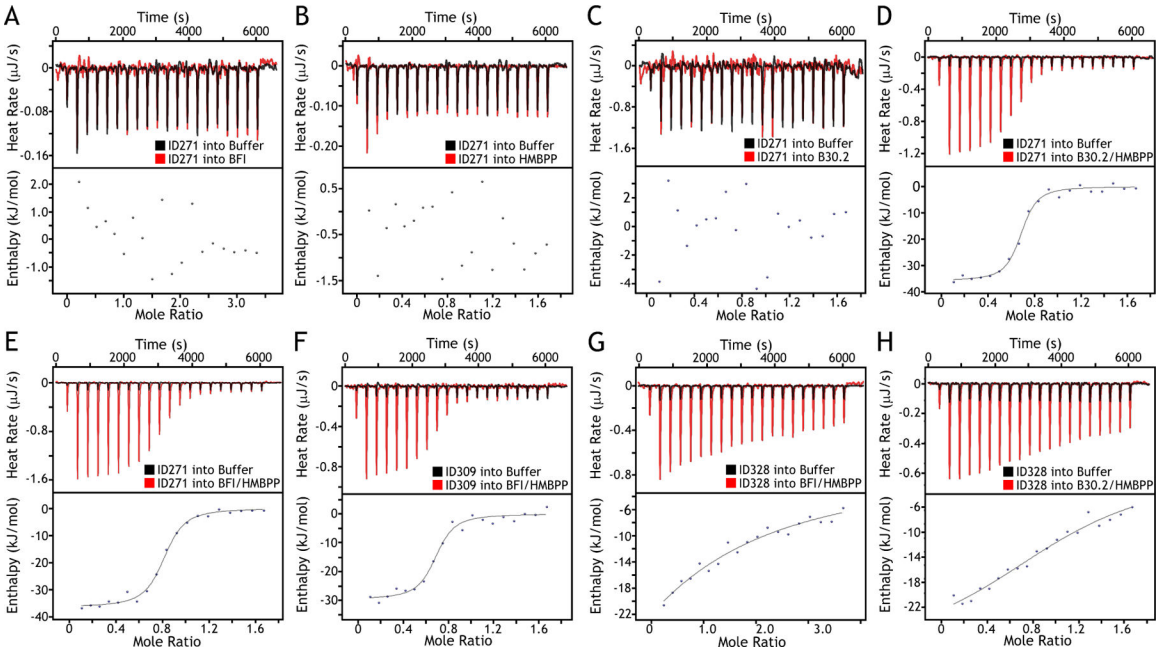

Figure 4. ITC titrations of BTN2A1 into HMBPP-bound BTN3A1 show a protein-protein interaction only in the presence of HMBPP.

A) Titrations of 400 μM BTN2A1 ID271 into buffer or into 40 μM BTN3A1 BFI. B) Titrations of 400 μM BTN2A1 ID271 into buffer or into 80 μM HMBPP. C) Titrations of 300 μM BTN2A1 ID271 into buffer or into 60 μM BTN3A1 B30.2. D) Titrations of 300 μM BTN2A1 ID271 into buffer or into a mixture of 60 μM BTN3A1 B30.2 and 120 μM HMBPP. E) Titrations of 400 μM BTN2A1 ID271 into buffer or into a mixture of 80 μM BTN3A1 BFI and 160 μM HMBPP. F) Titrations of 300 μM BTN2A1 ID309 into buffer or a mixture of 60 μM BTN3A1 BFI and 120 μM HMBPP. G) Titrations of 300 μM BTN2A1 ID328 into buffer or a mixture of 60 μM BTN3A1 BFI and 120 μM HMBPP. H) Titrations of 300 μM BTN2A1 ID328 into buffer or a mixture of 60 μM BTN3A1 B30.2 and 120 μM HMBPP. See also Figure S1.

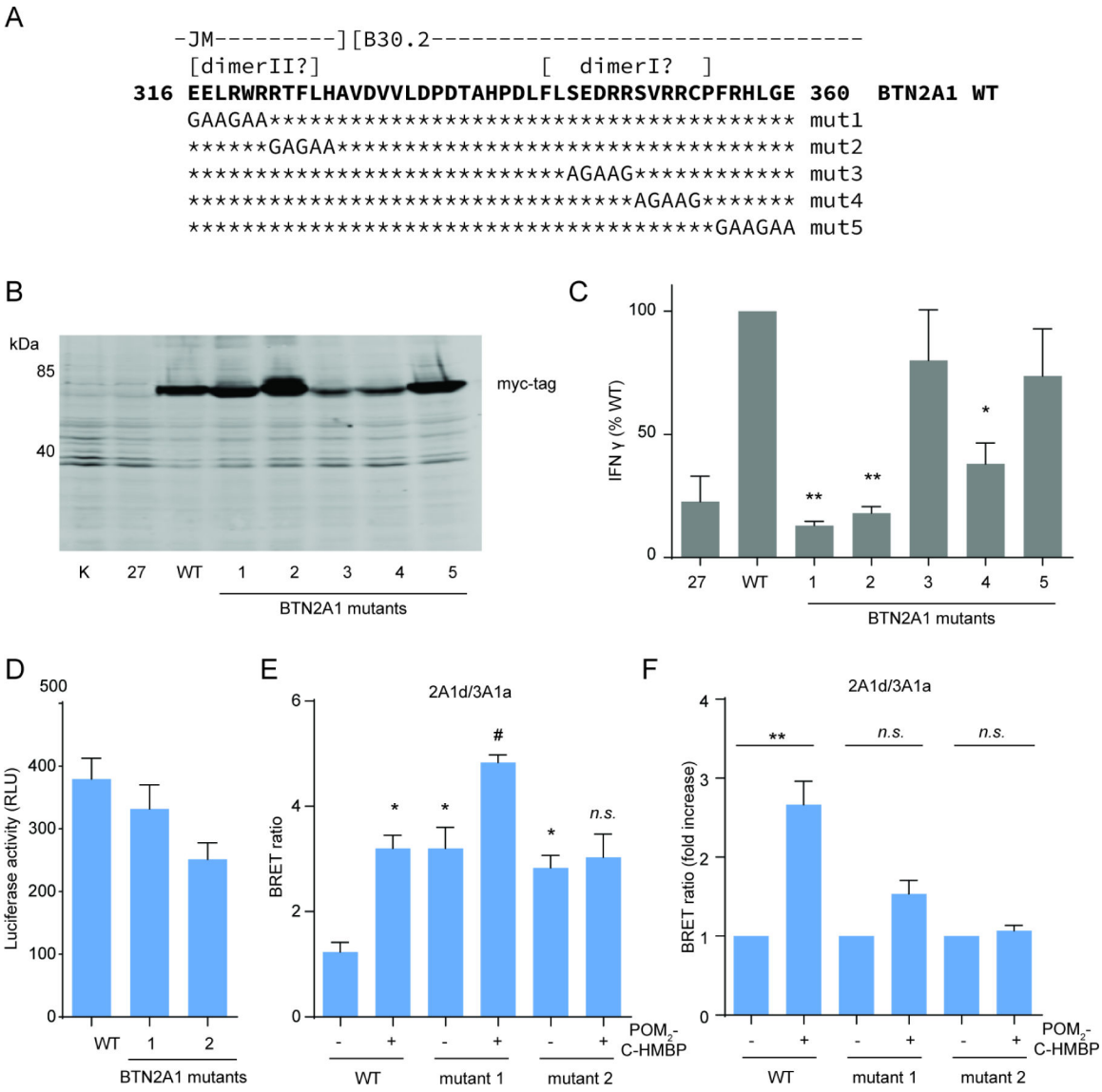

Figure 5. Regional mutations to the BTN2A1 internal domain abrogate pAg response.

A) Sequence of BTN2A1 at the intersection of the JM region and the B30.2 domain and regional mutations. Regions of BTN2A1 homologous to regions of BTN3A1 involved in dimer I or II are indicated. B) Western blot analysis of BTN2A1 expression. Proteins were visualized using anti-myc tag antibody. C) Impact of BTN2A1 mutations on interferon γ production in clone 27 K562 cells. Statistical significance was determined by one-way ANOVA with Tukey's post-hoc analysis. *$p < 0.05$ versus WT control, **$p < 0.01$ versus WT control. D) Luciferase readings from K562 cells transiently transfected with WT BTN2A1 versus mutants 1 and 2 (n=3). E) BRET ratios for WT K562 cells transfected with WT or mutant BTN2A1 as the donor and BTN3A1 as the acceptor following overnight treatment with POM_2-C-HMBP (1 μM) (n=3). Statistical significance was determined by one-way ANOVA with Tukey's post-hoc analysis. *$p < 0.05$ relative to the untreated WT control, $^{\#}p<0.05$ relative to the treated WT control. F) BRET ratios from prior panel normalized to the untreated control for each mutant to show the fold increase. Statistical

significance was determined by one-way ANOVA with Tukey's post-hoc analysis. **$p < 0.01$ versus corresponding control. Columns in bar graphs represent the mean ± SEM. See also Figures S2 and S3.

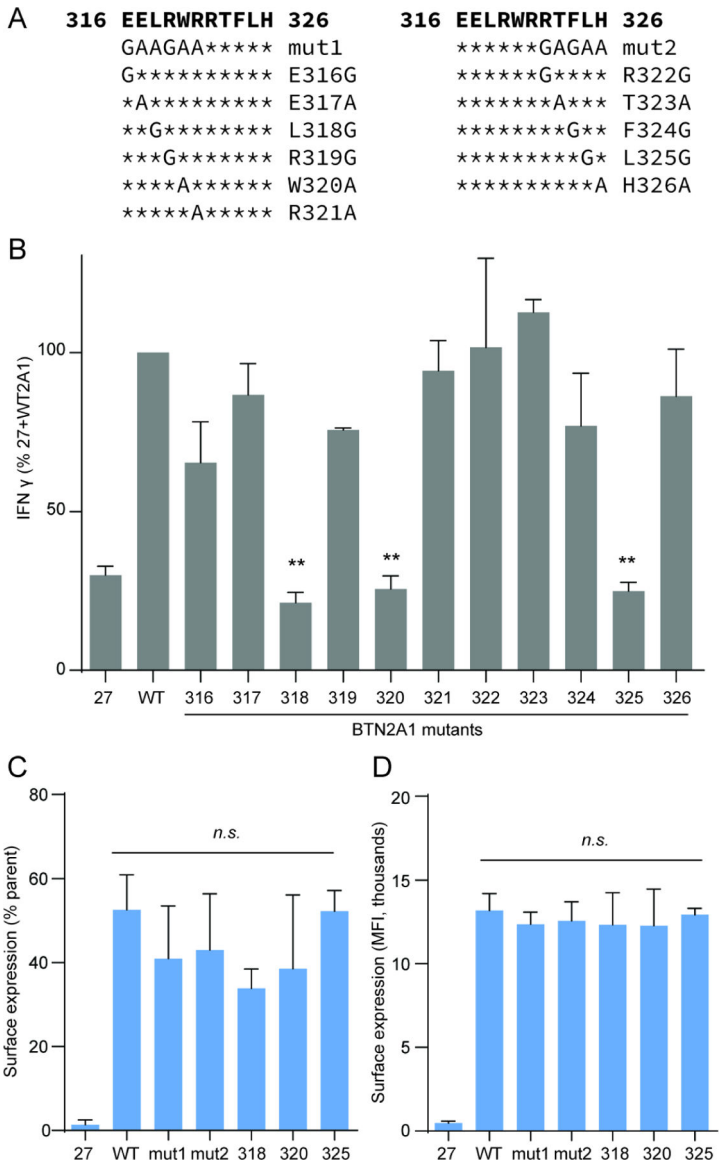

Figure 6. Individual mutations to the BTN2A1 internal domain within the putative dimer II interface abrogate pAg response.

A) Sequence of BTN2A1 at the putative dimer II interface showing regional mutations 1 and 2 and single amino acid mutations. B) Impact of BTN2A1 mutations on interferon γ production in clone 27 K562 cells. Statistical significance was determined by one-way ANOVA with Tukey's post-hoc analysis. **$p < 0.01$ versus 27+WT2A1 control. Columns represent the mean ± SEM. C,D) Surface expression of the inactive BTN2A1 mutants. Mutations were regenerated on extracellular 6x-his-tagged BTN2A1. Proteins were quantified by flow cytometer using anti-his-tag antibody. Data is presented as % of parent (FSC/SSC gated clone 27 cells) and mean fluorescence intensity of his-tag+ cells. Columns represent the mean ± STDEV. Statistical significance was determined by one-way ANOVA with Tukey's post-hoc analysis.

Table 1.

ITC titrations of BTN2A1 into HMBPP-bound BTN3A1[1]

Titrand	Titrant	Kd (μM)	n	ΔH (kJ/mol)	ΔS (J/mol*K)
BFI + HMBPP	ID271	0.886 ± 0.165	0.742 ± 0.123	−34.94 ± 4.79	−1.20 ± 15.40
BFI + HMBPP	ID309	0.674 ± 0.159	0.769 ± 0.243	−34.21 ± 5.41	3.56 ± 18.65
B30.2 + HMBPP	ID271	0.463 ± 0.088	0.611 ± 0.058	−36.15 ± 0.74	0.06 ± 4.07

[1]The binding parameters obtained by independent fit from NanoAnalyze are shown above for a series of titrations BTN2A1 constructs into BTN3A1. No data is shown for ID328 as the curves could not confidently be fitted. The number of repetitions, n, for each set is 7, 5, and 2 for BFI/ID271, BFI/ID309, and B30.2/ID271, respectively.

Key resources table

REAGENT or RESOURCE	SOURCE	IDENTIFIER
Antibodies		
anti-His Tag	Biolegend	Cat#362603
Myc-Tag Antibody	Cell Signaling Technology	Cat#2272S
Biological samples		
Unpurified Buffy Coat (25–50 mL)	Research Blood Components	Item#002
Chemicals, peptides, and recombinant proteins		
Human IL-2 IS, premium grade 50 μg	Miltenyi	Cat#130–097-745
HMBPP (HDMAPP ammonium salt)	Cayman chemical	Cat#13580
POM2-C-HMBP	(Hsiao et al., 2014)	N/A
BTN3A1 BFI	(Hsiao et al., 2014)	N/A
BTN3A1 B30.2	(Hsiao et al., 2014)	N/A
BTN2A1 ID271	This paper	N/A
BTN2A1 ID309	This paper	N/A
BTN2A1 ID328	This paper	N/A
Critical commercial assays		
TCRγ/δ+T Cell Iso Kit, human	Miltenyi	Cat#130–092-892
ELISA MAX™ Standard Set Human IFN-γ	Biolegend	Cat#430101
Nano-BRET PPI starter kit (618 ligand probe and luciferin substrate)	Promega	Cat#N1811
Experimental models: Cell lines		
K562 cells	Millipore Sigma	Cat#89121407–1VL
K562 cells - ΔBTN2A1 clone 1	This paper	N/A
K562 cells - ΔBTN2A1 clone 27	This paper	N/A
Oligonucleotides		
Please refer to Table S1 for sequences	IDT	N/A
Recombinant DNA		
pcDNA3.1 (+)	Invitrogen	Cat#V790–20
pET-21b	Novagen	Cat#69741–3
pX335-U6-Chimeric_BB-CBh-hSpCas9n (D10A)	Addgene	Cat#42335
Nano-BRET PPI starter kit (pHTC HaloTag CMV-neo and pNLF1-C [CMV/Hygro])	Promega	Cat#N1811
pX335-U6-Chimeric_BB-CBh-hSpCas9n (D10A) - BTN2A1 sense	This paper	N/A

REAGENT or RESOURCE	SOURCE	IDENTIFIER
pX335-U6-Chimeric_BB-CBh-hSpCas9n (D10A) - BTN2A1 antisense	This paper	N/A
pcDNA3.1 (+) - BTN2A1-myc	This paper	N/A
pcDNA3.1 (+) - BTN2A1-myc ΔID	This paper	N/A
pcDNA3.1 (+) - BTN2A1-myc - mut1	This paper	N/A
pcDNA3.1 (+) - BTN2A1-myc - mut2	This paper	N/A
pcDNA3.1 (+) - BTN2A1-myc - mut3	This paper	N/A
pcDNA3.1 (+) - BTN2A1-myc - mut4	This paper	N/A
pcDNA3.1 (+) - BTN2A1-myc - mut5	This paper	N/A
pcDNA3.1 (+) - BTN2A1-myc - E316G	This paper	N/A
pcDNA3.1 (+) - BTN2A1-myc - E317A	This paper	N/A
pcDNA3.1 (+) - BTN2A1-myc - L318G	This paper	N/A
pcDNA3.1 (+) - BTN2A1-myc - R319G	This paper	N/A
pcDNA3.1 (+) - BTN2A1-myc - W320A	This paper	N/A
pcDNA3.1 (+) - BTN2A1-myc - R321A	This paper	N/A
pcDNA3.1 (+) - BTN2A1-myc - R322G	This paper	N/A
pcDNA3.1 (+) - BTN2A1-myc - T323A	This paper	N/A
pcDNA3.1 (+) - BTN2A1-myc - F324G	This paper	N/A
pcDNA3.1 (+) - BTN2A1-myc - L325G	This paper	N/A
pcDNA3.1 (+) - BTN2A1-myc - H326A	This paper	N/A
pcDNA3.1 (+) - 6xHis-BTN2A1	This paper	N/A
pcDNA3.1 (+) - 6xHis-BTN2A1 - mut1	This paper	N/A
pcDNA3.1 (+) - 6xHis-BTN2A1 - mut2	This paper	N/A
pcDNA3.1 (+) - 6xHis-BTN2A1 - L318G	This paper	N/A
pcDNA3.1 (+) - 6xHis-BTN2A1 - W320A	This paper	N/A
pcDNA3.1 (+) - 6xHis-BTN2A1 - L325G	This paper	N/A
pHTC HaloTag CMV-neo - BTN2A1	This paper	N/A
pHTC HaloTag CMV-neo - BTN3A1	This paper	N/A
pNLF1-C [CMV/Hygro] - BTN2A1	This paper	N/A
pNLF1-C [CMV/Hygro] - BTN2A1 - mut1	This paper	N/A
pNLF1-C [CMV/Hygro] - BTN2A1 - mut2	This paper	N/A
pNLF1-C [CMV/Hygro] - BTN3A1	This paper	N/A
pET-21b - BTN2A1 - ID271	This paper	N/A
pET-21b - BTN2A1 - ID309	This paper	N/A
pET-21b - BTN2A1 - ID328	This paper	N/A
Software and algorithms		
GraphPad Prism 6	GraphPad	www.graphpad.com/
NanoAnalyze	TA instruments	www.tainstruments.com
NMRPipe	NMRbox	www.nmrbox.org

REAGENT or RESOURCE	SOURCE	IDENTIFIER
CcpNmr	NMRbox	www.nmrbox.org
Other		
Lymphocyte Separation Media	Corning	Cat#MT25072CV